Climate Dynamics (2023) 60:3613–3628
https://doi.org/10.1007/s00382-022-06483-y

Influence of boreal spring sea surface temperature anomalies over the tropical South Atlantic on the Meiyu onset

Shaoyu Zhang[1,2] · **Yimin Liu**[1,2] · **Chen Sheng**[1,2] · **Tingting Ma**[1]

Received: 5 May 2022 / Accepted: 27 August 2022 / Published online: 18 October 2022

Abstract
This study investigates the impact of boreal spring tropical South Atlantic surface sea temperature anomalies (TSA-SSTA) on the anticyclone over the western North Pacific (WNPAC) and the Meiyu onset date (MOD) based on reanalysis data and numerical experiments. The results indicate an intimate linkage between the MOD and TSA-SSTA, in which warmer spring TSA-SSTA are associated with an earlier MOD and vice versa, and the underlying mechanism is identified. Warm TSA-SSTA can trigger a Gill-type response and anomalous equatorial Walker circulation, which leads to anomalous upward motion and latent heating over the Maritime Continent. This anomalous condition over the Maritime Continent strengthens local Hadley circulation accordingly accompanied by anomalous descending motion over the western North Pacific. This descending motion reduces the local rainfall and enhances the equatorward northerly wind at low level. Further analysis reveals that local Sverdrup positive feedback between the anomalous diabatic cooling owing to reduced rainfall and the lower-level equatorward northerly wind is critical for sustaining the well-developed anomalous WNPAC. The abundant water vapor transport embedded in the northwestern flank of the anomalous WNPAC eventually favors an earlier MOD. Atmospheric conditions corresponding to cold TSA-SSTA produce the opposite effect. The spring TSA-SSTA can therefore prominently communicate with the subsequent East Asian MOD via the aforementioned mechanism, and the spring TSA-SSTA can be interpreted as a precursor signal of the East Asian MOD.

Keywords Meiyu onset · Tropical South Atlantic · Western North Pacific anticyclone · East Asian summer monsoon

1 Introduction

Meiyu (Changma or Baiu) is an important weather and climate phenomenon in East Asia during the boreal summer (Tao 1987; Ding et al. 2007; Ding 2020). As the major rainfall belt of the summer monsoon, Meiyu exerts a great impact on East Asian countries including China, Japan, and Korea (Ninomiya and Muraki, 1986; Ding 1992, 2007; Kubota et al. 2016), which are densely populated and home to approximately one-fifth of the global population (Zhou et al. 2019). Extreme rainfall events occur frequently in the Meiyu season, which strongly influence agriculture, socio-economic development, and societal activity over the middle and lower Yangtze River Valley (MLYRV) (Zhu et al. 2008; Gao et al. 2011). Previous studies have suggested that the Meiyu onset date (MOD) is a critical factor that controls the total rainfall and duration of the full Meiyu season (e.g., Wei and Zhang 2004; Huang et al. 2012). An earlier MOD favors a longer Meiyu duration and more rainfall, while a later MOD favors a shorter Meiyu duration and less rainfall. The MOD has therefore attracted considerable attention given its utility for predicting subsequent weather conditions and anomalies.

Previous studies found that ocean forcings are of great importance to MOD variations besides circulation factors such as the East Asian upper-level jet and subtropical high (Lu et al. 2001; Li et al. 2018), the Northeast China cold

*Corresponding author:Yimin Liu and Chen Sheng

✉ Yimin Liu
lym@lasg.iap.ac.cn

✉ Chen Sheng
shengchen@lasg.iap.ac.cn

[1] State Key Laboratory of Numerical Modeling for Atmospheric Sciences and Geophysical Fluid Dynamics (LASG), Institute of Atmospheric Physics, Chinese Academy of Sciences, 100029 Beijing, China

[2] College of Earth and Planetary Sciences, University of Chinese Academy of Sciences, 100049 Beijing, China

vortex (Wang et al. 2010), the East Asian winter monsoon (Hu et al. 2014), and the South Asian high (Li et al. 2019a). For example, several studies demonstrated that the El Niño-Southern Oscillation (ENSO) in the Pacific had an influence on MOD (Zhao 1996; Gao et al. 2011). By comparing with the eastern Pacific (Niño3 region), Wang et al. (2009) indicated that the central Pacific (Niño4 region) sea surface temperature (SST) anomalies exert a more significant impact on the MOD, in which a warm (cold) ENSO favors a later (earlier) MOD by altering the water vapor transport. Yao et al. (2019) highlighted the role of different ENSO types with regard to MOD variations, and suggested that a warm ENSO in the eastern Pacific (central Pacific) winter could result in strong (weak) intra-seasonal oscillation over the western North Pacific, thus leading to an earlier (later) MOD. Sea surface temperatures in the Indian Ocean, as a capacitor that can sustain ENSO effects, in May favor the establishment of an earlier Indian summer monsoon and thus influences the subsequent MOD (Yao et al. 2019). Previous research has shown that SST anomalies over the North Atlantic could trigger a Rossby wave train and thereby influence MOD variations (Xu et al. 2001; Wang and Qian 2005; Zhu et al. 2008). Warm SST anomalies over the North Atlantic in the preceding winter tend to favor an earlier MOD and vice versa.

Several studies have addressed MOD variations in terms of SST forcing signals that span from the tropical Pacific, Indian, and North Atlantic oceans. There is also a prominent signal over the tropical South Atlantic (TSA) (e.g., Wang and Qian 2005), but further insight is presently limited. To address this knowledge gap, the present study focuses on the TSA. Previous statistical analysis and model experiments have demonstrated a close linkage between tropical Atlantic SST and East Asia climate (e.g., Jin and Huo 2018; Choi and Ahn 2019; Yuan and Yang 2020; Qiu et al. 2021). However, it should be noted that the SST over the tropical North Atlantic and TSA belong to different major empirical orthogonal function modes (Huang et al. 2004; Handoh et al. 2006a, b), which means that SST variations over the tropical North Atlantic and TSA are relatively independent of each other (Enfield et al. 1999). The tropical North Atlantic has been recognized as an important source in regulating the East Asian climate (Rong et al. 2010; Li et al. 2019b; Chen et al. 2018; Liu et al. 2020a; Qiu et al. 2021) and the variation of the MOD (Xu et al. 2001; Wang and Qian 2005; Zhu et al. 2008). However, climate effects of the TSA have received scarce attention in the literature and are therefore worth a deep investigation. To date, it remains unclear whether and how the TSA affects the MOD.

The aims of present study are to identify the interannual impact of SST anomalies over the TSA (TSA-SSTA) on the MOD and investigate the underlying mechanism. The remainder of this paper is as follows. Section 2 presents the data, methods, and model. Section 3 presents the relationship between TSA-SSTA and the MOD. Section 4 investigates the possible mechanism using numerical models. A conclusion and discussion including the multi-regression equation are given in Sect. 5.

2 Data, method and models

2.1 Data

This study uses monthly mean data from the MERRA2 reanalysis product (Rienecker et al. 2011) and SST data from the Extended Reconstructed Sea Surface Temperature, version 5 (ERSSTv5) dataset (Huang et al. 2017). Precipitation data are from the Global Precipitation Climatology Project (GPCP V2.3) (Adler et al. 2018), which merges observations and satellite precipitation data. The outgoing longwave radiation (OLR) data is obtained from National Oceanic and Atmospheric Administration (Liebmann and Smith 1996). Observational precipitation data are also used from 824 stations in China provided by the Chinese Meteorological Information Center (http://data.cma.cn/en/?r=site/index) to calculate the MOD. The ERA5 data (Hersbach et al. 2020) and COBESST (Ishii et al. 2005) are also used, and the results are generally consistent with the present study.

The research period in this study is 1980–2018. The horizontal resolutions of the MERRA2, NOAA ERSSTv5, and GPCP precipitation data are 1.25° × 1.25°, 2.0° × 2.0°, and 2.5° × 2.5°, respectively.

The indices used in this paper include Niño4, Niño3, Niño3.4, NTA (North Tripole Atlantic SST), NAO (North Atlantic Oscillation), TNA (Tropical Northern Atlantic Index), and PNA (Pacific North American pattern), which are obtained from https://psl.noaa.gov/data/climateindices/list/. The Indian Ocean dipole mode index (DMI; Saji et al. 1999) is calculated as the difference between area-averaged SST anomalies in the western pole (10° S–10° N, 50° E–70° E) and eastern pole (10° S–0°, 90° E–110° E). The Indian Ocean basin uniform mode (IOBM) index is the time series of the first empirical orthogonal function mode of tropical Indian Ocean SST (Zhao et al. 2018).

The monthly data in March, April, and May (MAM) are used to calculate the seasonal mean during boreal spring. To focus on the interannual variability, the linear trend and decadal variation (>9 years) are removed from all raw data sets and indices.

2.2 Method

Following Chen and Zhao (2000) and Ding et al. (2007), the definition of the Meiyu onset date (MOD) is based on the daily total precipitation in a group of stations over the MLYRV. This group consists of five gauges including Shanghai (31°24′ N, 121°27′ E), Nanjing (32°00′ N, 118°48′ E), Wuhan (30°37′ N, 114°08′ E), Jiujiang (29°44′ N, 116°00′ E), and Wuhu (31°20′ N, 118°23′ E). The details of the definition of the MOD are as follows. First, a rainy day is identified when the daily total precipitation in a group exceeds 10 mm and the number of stations with daily precipitation exceeding 0.1 mm is more than one. Second, if the number of rainy days is greater than five in a successive 10-day period, the first single rainy day is identified as the MOD. The Meiyu onset date index (MODI) is defined as the normalized time series of the MOD. A positive MODI phase indicates that the MOD is later than normal and vice versa.

The TSA-SSTA index (TSAI) is defined as the normalized time series of the averaged SST over the TSA region addressed in this study. This defined region is enclosed by 25°S–0° and 30°W–15°E. A positive TSAI phase indicates that the area-averaged TSA-SSTA is warm and vice versa.

To examine the water vapor transport anomalies related to the MOD, we calculate the horizontal water vapor flux (WVF), $WVF = \frac{1}{g}\overrightarrow{V}q = (\frac{1}{g}uq, \frac{1}{g}vq)$, where q is the specific humidity, $\overrightarrow{V} = (u, v)$ is the horizontal wind, and g is the gravitational acceleration.

This study applies statistical methods including correlation, partial correlation, and linear regression. The two-tailed Student's t-test is used to determine the statistical significance.

2.3 Models

Atmospheric moisture backward trajectory simulations are conducted based on the Hybrid Single-Particle Lagrangian Integrated Trajectory (HYSPLIT) 5.0 model (Stein et al. 2015) to explore the variation of the MLYRV moisture source in June. The modeling period is from 00:00 UTC on June 1 until 00:00 UTC on June 30 for each year from 1980 to 2018 with an integration time interval of 6 h. The target region is the MLYRV, which is portioned into 45 points as starting parcels. The parcels are released at 500, 1000, and 1500 m (850 hPa) above ground level. The 16,200 trajectories are derived each year based on the product of the numbers of horizontal points (45), the vertical levels (3) and the times (30days×24 h/6 h). The average duration of moisture persistence in the atmosphere is approximately 10 days (Trenberth et al. 1998, 1999), and the model is less accurate when the integration duration is more than 11 days (Jiang et al. 2013). The backward trajectories are therefore integrated over 10 days (240 h) for each grid site. Following Liu et al. (2020b), the variation of the moisture source is determined by analyzing the specific humidity along the backward trajectories.

The linear baroclinic model (LBM) (Watanabe and Kimoto 2000) is applied to investigate the feedback influence of the anomalous diabatic heating on circulation. The model used in this study has 20 σ levels and T42 horizontal resolution. More details regarding the model description are given in Watanabe and Jin (2003). The LBM is a time-varying model that linearizes the basic state based on primitive equations. We take climatology in June as the basic state in this study. A 30-day integration for each experiment is conducted. Because the model reaches its steady state after approximately 14 days, the results averaged over 15–30 days are shown here.

Numerical experiments to investigate the influence of TSA-SSTA on the general circulation are conducted based on the Community Earth System Model, version 1.2.0 (CESM1.2.0). The land component is the community land model, version 4.0 (Oleson et al. 2010); the oceanic component is the parallel ocean program, version 2.0 (Smith and Gent 2010); the sea ice component is the Los Alamos sea ice model, version 4.0 (Hunke and Lipscomb 2008); and the atmospheric component is the community atmospheric model, version 4.0 (CAM4, Neale et al. 2013). For more details, see http://www.cesm.ucar.edu/models/cesm1.2/. The horizontal resolution of the atmospheric component (CAM4) of CESM1.2.0 in this study is approximately 2°. The number of vertical levels is 26 extending from the surface to 3.5 hPa. Two atmospheric general circulation model (AGCM) experiments based on CAM4 are conducted, as presented in Sect. 4.3.

3 Relationship between the MOD and TSA-SSTA

The correlations between the MODI and spring global SST anomalies are shown in Fig. 1a. A significant positive correlation appears over the tropical central eastern Pacific, and negative correlation coefficients spread across its flanks in a K-shape. This anomalous horseshoe-shaped SST pattern over the Pacific closely resembles a warm Central Pacific type ENSO pattern. We calculate the correlation between the MODI (defined in Sect. 2.2) and spring Niño4 and find that a coefficient of 0.32 passes the 0.1 significance level. These results suggest that the Meiyu onset is significantly affected by ENSO events (Wang and Qian, 2005; Wang et al., 2009; Yao et al. 2019). A positive correlation is evident over the Indian Ocean in association with the warm ENSO, especially in the southwestern Indian Ocean. There is also

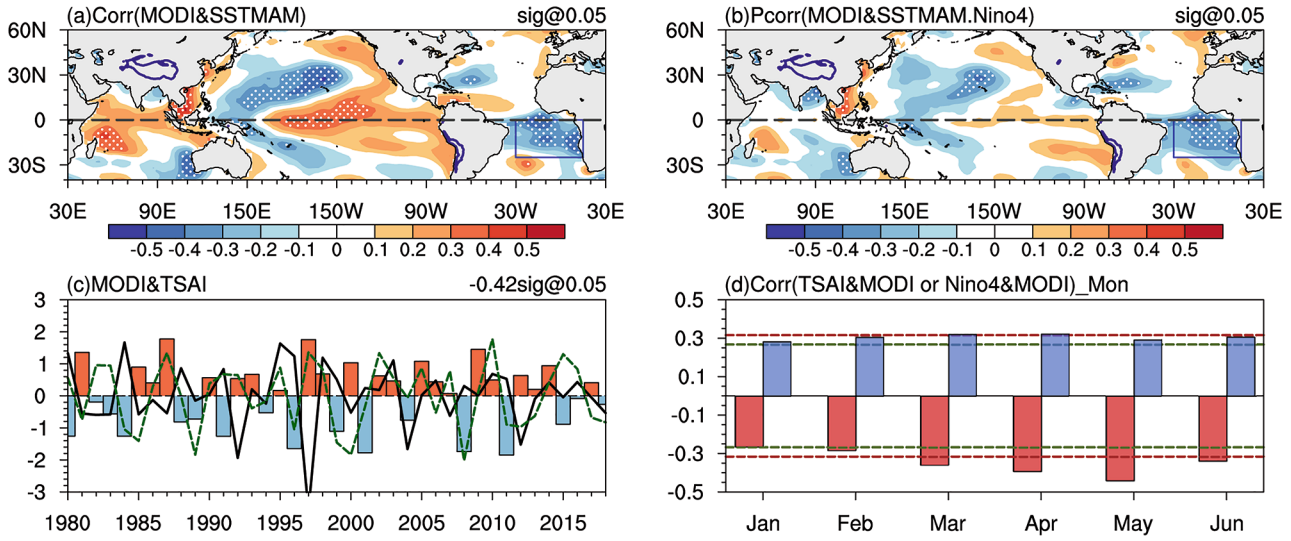

Fig. 1 (a) Spatial distribution of the correlation coefficients between the MODI and spring sea surface temperature anomalies. (b) Same as (a), but for the partial correlation coefficients with the spring Niño4 index is removed. The dots in (a) and (b) indicate the area exceeding the 0.05 significance level. The blue rectangle marks the TSA region. (c) Normalized time series of the MODI (bar), TSAI (black line) and Niño4 (green dash line) in MAM. (d) Correlation coefficient between the monthly TSAI (red bar) and MODI and that between Niño4 (blue bar) the MODI. The green (red) dashed line denotes that the correlations are significant at the 0.1 (0.05) significance level

a uniform mode with significant negative correlation coefficients occurring over the TSA. This signal was also detected in an early study by Wang and Qian (2005), and suggests an intimate linkage between the MOD variability and TSA-SSTA. To exclude the ENSO's effects, Fig. 1b presents the partial correlation between the MODI and SST by removing the spring Niño4 index. A comparison with Fig. 1a clearly shows that the Central Pacific type ENSO signal and Indian Ocean capacitor signal are insignificant, but that the significantly negative correlation coefficients over the TSA remain nearly unchanged. This is mainly because the concurrent spring correlation between TSA-SSTA and the Niño4 index is low (only −0.07, not shown in the figure). These statistical results imply that the relationship between the MOD and spring TSA-SSTA is unrelated to the spring ENSO, which is consistent with the previous findings (Chang et al. 2006; Kucharski et al. 2007; Sheng et al. 2022). Moreover, the TSA-SSTA pattern (Fig. 1a, b) bears great resemblance to the major variation mode of the SSTA over the tropical Atlantic (Huang et al. 2004). Therefore, the TSA-SSTA is considered as a potential independent driver that contributes to the interannual variation of the MOD.

The time series of the MODI and TSAI (defined in Sect. 2.2) is shown in Fig. 1c. The correlation coefficient between the MODI and spring TSAI is −0.42, passing the 0.05 significance level. When the spring Niño4 is linearly removed, the robust correlation coefficient between the MODI and spring TSAI remains almost unchanged (−0.417, not shown in the figure). Figure 1d shows the lead-lag correlation between the MODI and TSAI and Niño4. It is evident that the coefficients between the MODI and TSAI are significant throughout the entire spring and can sustain until the following June owing to the oceanic thermal memory (Fig. 1d). The above results thus further verify the close linkage between the spring TSA-SSTA and MOD. Positive spring TSA-SSTA favor an earlier MOD, while negative spring TSA-SSTA favor a later MOD. The teleconnection between the TSA and East Asia is presented in the following section.

3.1 Water vapor conditions

Because the MOD is determined by the rainfall, and because the rainfall is closely linked to the water vapor transport, we use HYSPLIT to show the backward trajectory of the water vapor source in June in the climate mean state (Fig. 2a and b) and in the positive TSAI phase (Fig. 2c and d). The climatological water vapor sources (Fig. 2a) regarding the Meiyu onset are located in the northern Indian Ocean, South China Sea, and the western North Pacific, which is generally consistent with previous findings (e.g., Yang et al. 2014). The water vapor sources in these regions (Fig. 2b) are concentrated at lower levels. There is also some water vapor from the westerly jet at middle to upper levels (Fig. 2b), but the amount along this path is relatively small (Fig. 2a). This result suggests that the three major water vapor sources are related to the Meiyu onset, including the northern Indian Ocean, South China Sea, and western North Pacific.

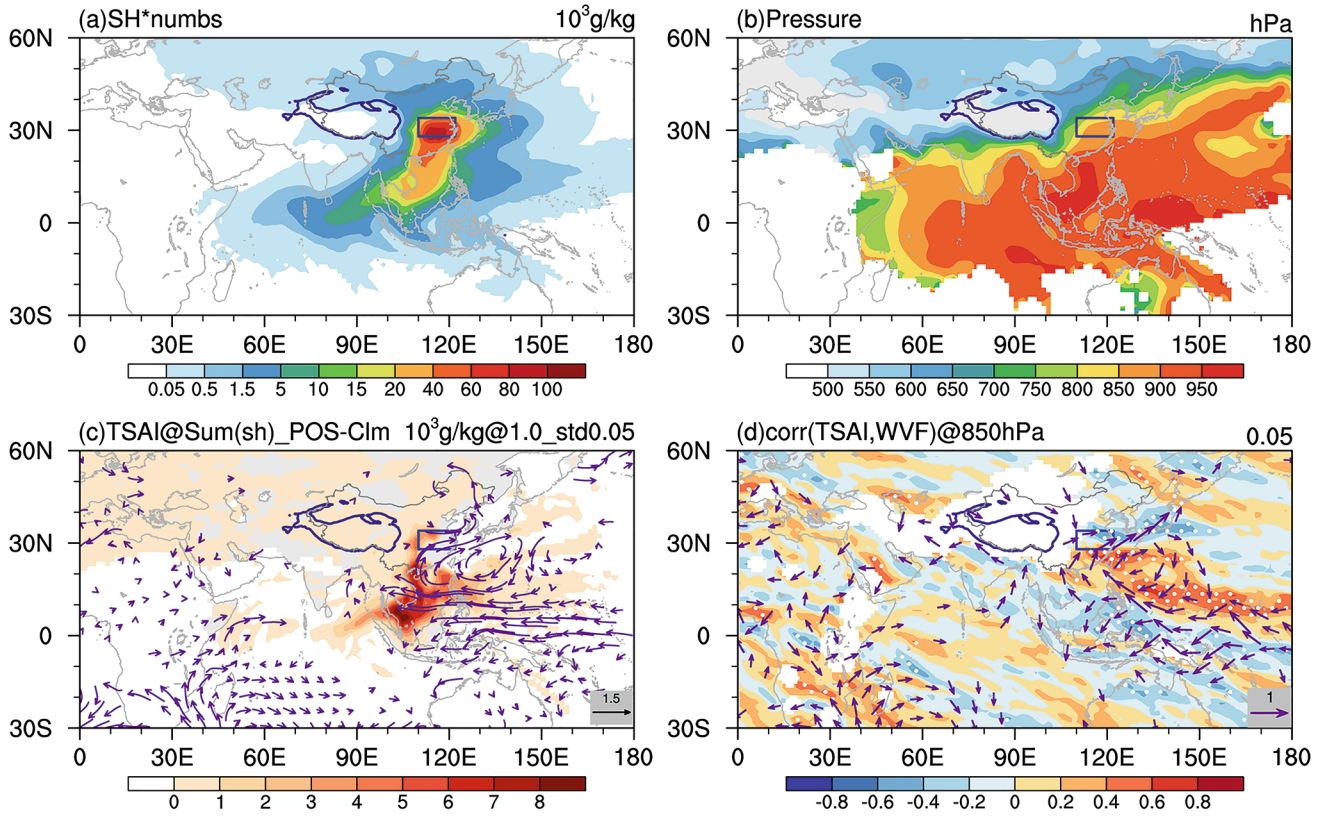

Fig. 2 (a) Climate mean of the number of particles weighted by the specific humidity (shading; units: kg/kg) in June arriving in the domain of the MLYRV for day − 10. (b) Same as (a) but shows the particle pressure (units: hPa). (c) Difference between the positive TSAI phase (greater than 1.0 standard deviation) and climatology of the number of particles weighted by the specific humidity (shading; units: kg/kg) in June arriving in the domain of the MLYRV for day − 10 and an 850-hPa WVF (vectors). (d) Correlation between the TSAI and 850-hPa WVF (vectors) and its divergence (shading). The purple arrows and dots in (c) and (d) indicate variables exceeding the 0.05 significance level

Figure 2c shows the trajectories of water vapor in the positive TSAI phase. It is clear that the anomalous water vapor over the MLYRV coming from the northern Indian Ocean is not prominent in the positive TSAI phase. However, water vapor coming from the South China Sea and western North Pacific is evident. The WVF and its divergence are shown in Fig. 2d. This anomalous anticyclonic WVF (Fig. 2d) could enhance the climatology transport of water vapor from the western North Pacific and South China Sea and converge water vapor over the MLYRV, which is conducive to an earlier MOD. The results shown in Fig. 2d are in line with those in Fig. 2c, further supporting that the WNPAC in the positive TSAI phase is an important system that favors the transport of water vapor to the MLYRV. The negative TSAI phase corresponds to the opposite situation.

3.2 Circulation characteristics

Figure 3 shows that in June the horizontal circulation and geopotential height regressed upon the spring TSAI (Fig. 3a and b) and MODI multiplied by − 1 (Fig. 3c and d). The circulation anomalies revealed by the TSAI (Fig. 3a and b) closely resemble the typical circulation mode revealed by the MODI (Fig. 3c and d), indicating that the anomalous circulation triggered by TSA-SSTA (Fig. 3a and b) plays a critical role in the MOD anomaly. In the following discussion, unless otherwise specified, the circulation anomalies are particularly referred to those in June, which is the climatic Meiyu onset month. In the positive TSAI phase, there are two anomalous high centers embedded in the South Asia High at 200 hPa (Fig. 3a) over the western Tibetan Plateau and Japan, which might enhance the South Asian High and make it slightly northward shift. The divergent wind to the southwestern flank of the anomalous high centered in the upper level over Japan is conducive to the anomalous upward motion associated with the Meiyu onset over the MLYRV. The anomalous anticyclone circulation over the western North Pacific leads to a climatic WNPAC farther westward at 850 hPa (Fig. 3b). The south–westerly wind associated with the anomalous WNPAC will transport more

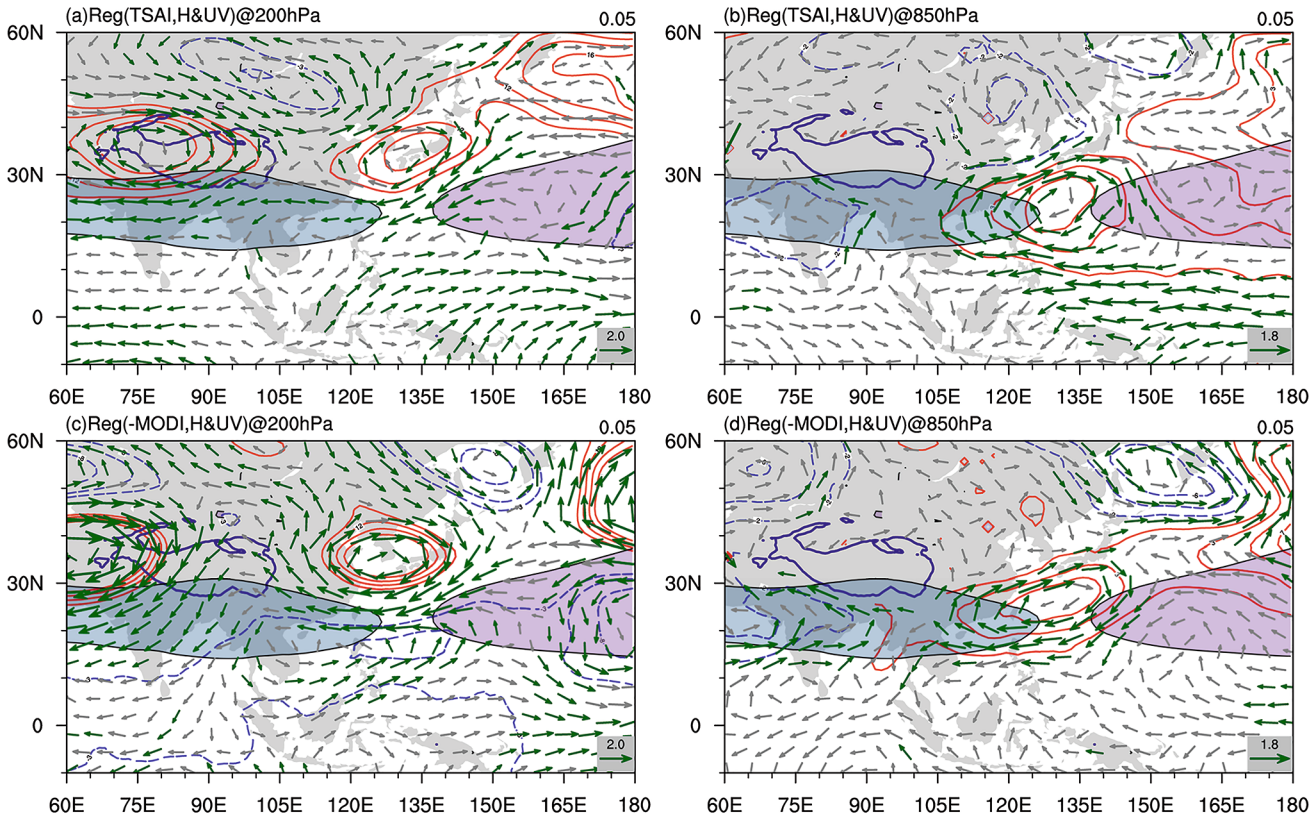

Fig. 3 (a) Regressed 200-hPa geopotential height (contours; units: gpm) and wind (vectors; units: m/s) on the TSAI in June. (b) Same as (a), but for 850 hPa. (c) and (d) Same as (a) and (b), respectively, but for the MODI. Contours exceeding the 0.05 significance level are shown. Vectors exceeding the 0.05 significance level are colored green. The climatic June geopotential height exceeding the 1520 gpm at 850 hPa and 12,500 gpm at 200 hPa are colored purple and blue, respectively

water vapor to the MLYRV (Fig. 2). As a result, the anomalous abundant water vapor and upward motion lead to an earlier Meiyu onset. In the negative TSAI phase, the situation is the opposite.

4 Possible mechanisms

The above results document that the abundant (deficient) water vapor and upward (downward) motion triggered by warm (cold) spring TSA-SSTA favor an earlier (later) MOD. In this section, we examine the possible mechanism by which spring TSA-SSTA affect the remote general circulation over East Asia.

4.1 Dynamical diagnosis

Figure 4a and b show the correlation between the TSAI and anomalous velocity potential and divergence wind at 200 and 850 hPa in June, respectively. Associated with TSA-SSTA, the anomalous divergence is observed over the tropical Atlantic and the Maritime Continent at 200 hPa (Fig. 4a). The anomalous convergence is evident over the tropical central western Pacific. The low-level pattern (Fig. 4b) is out of phase with its counterpart at the upper level (Fig. 4a). The anomalous rising and sinking motion implied by the vertical structure (Fig. 4a and b) is well matched with anomalous Walker circulation (Fig. 4c). Governed by the Gill response (Gill 1980; Hong et al. 2014) regarding diabatic heating, the anomalous westerlies (Fig. 4d) prevail to the west of the warming TSA, which enhances the anomalous ascending motion over the TSA region and changes the zonal Walker circulation along the equator (Fig. 4c) (Jin and Huo 2018). The low-level anomalous easterly wind (Fig. 4c and d) over the central Pacific is found to cause anomalous cooling SST over the central Pacific by enhancing the climatic easterly wind. The atmospheric responses along the tropical region are further maintained by Bjerknes positive feedback (Bjerknes 1969; Ham et al. 2013). The anomalous easterlies as well as the anomalous WNPAC (Fig. 4d) are consequently well organized over the tropical central western Pacific and western North Pacific.

It is noteworthy that the anomalous easterlies associated with anomalous Walker circulation are confined to the

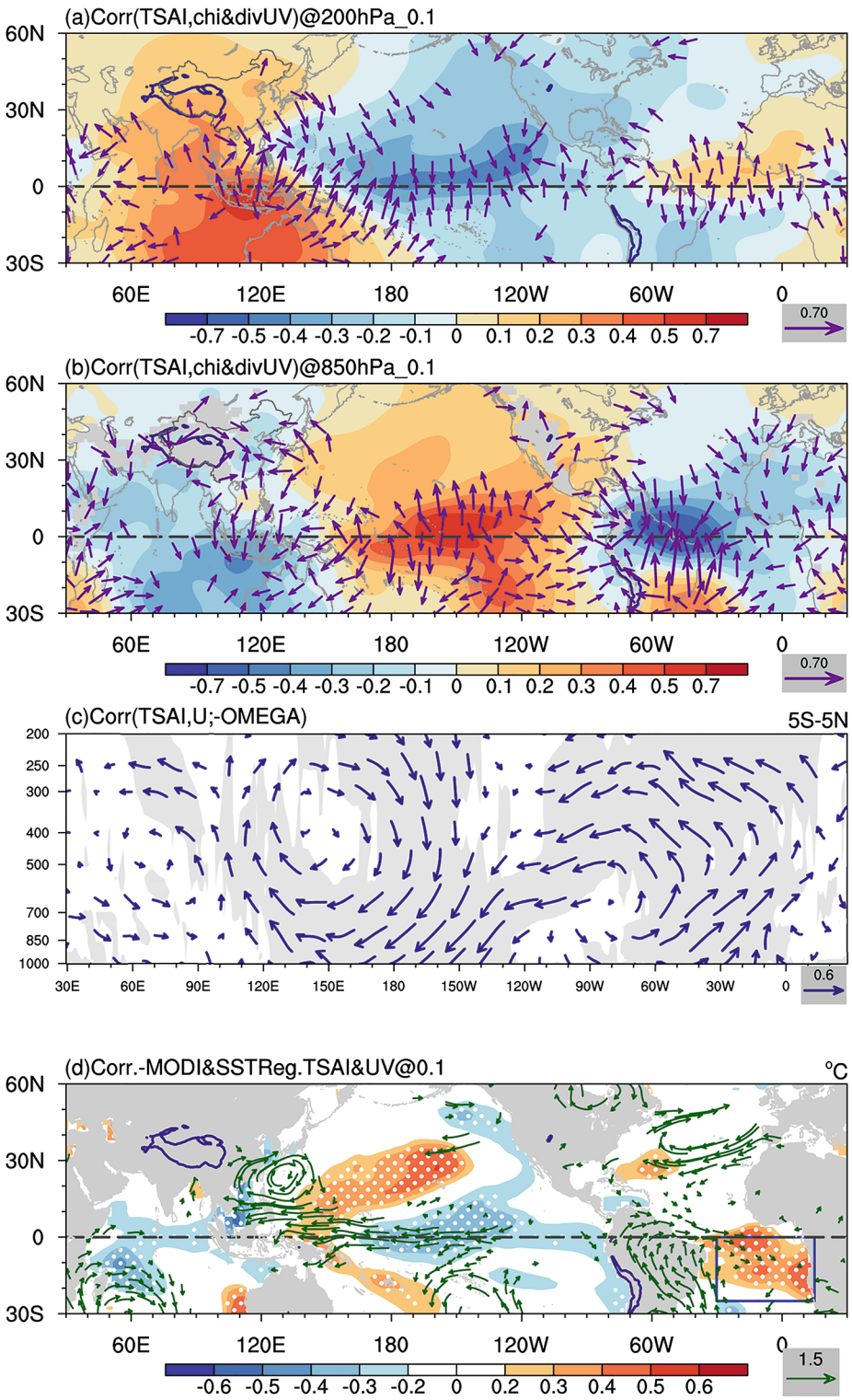

Fig. 4 Distribution of the correlation coefficients between the TSAI and (a) 200-hPa and (b) 850-hPa velocity potential fields (shading) and divergent wind (vectors) in June. The purple arrows exceed the 0.1 significance level. (c) Distribution of correlation coefficients between the TSAI and 5°S–5°N mean zonal vertical circulation (vectors). Vectors exceeding the 0.1 significance level are colored in gray shading. (d) Distribution of correlation coefficients between the MODI and spring SST anomalies (shading) and the regressed 850-hPa wind (vectors; units: m/s) in June on the TSAI. Areas in (d) exceeding the 0.1 significance level are colored as white dots. Anomalous horizontal winds exceeding the 0.1 significance level are shown as green vectors

equatorial central western Pacific. However, the reason why the anomalous subtropical anticyclone is well developed over the western North Pacific remains unclear and is further addressed later in the paper.

Figure 5 shows the correlation between the TSAI and rainfall (Fig. 5a) and OLR (Fig. 5b). A meridional dipole mode of diabatic heating centered at the Maritime Continent and western North Pacific is clear in Fig. 5a and b. Specifically, consistent with the anomalous rising motion over

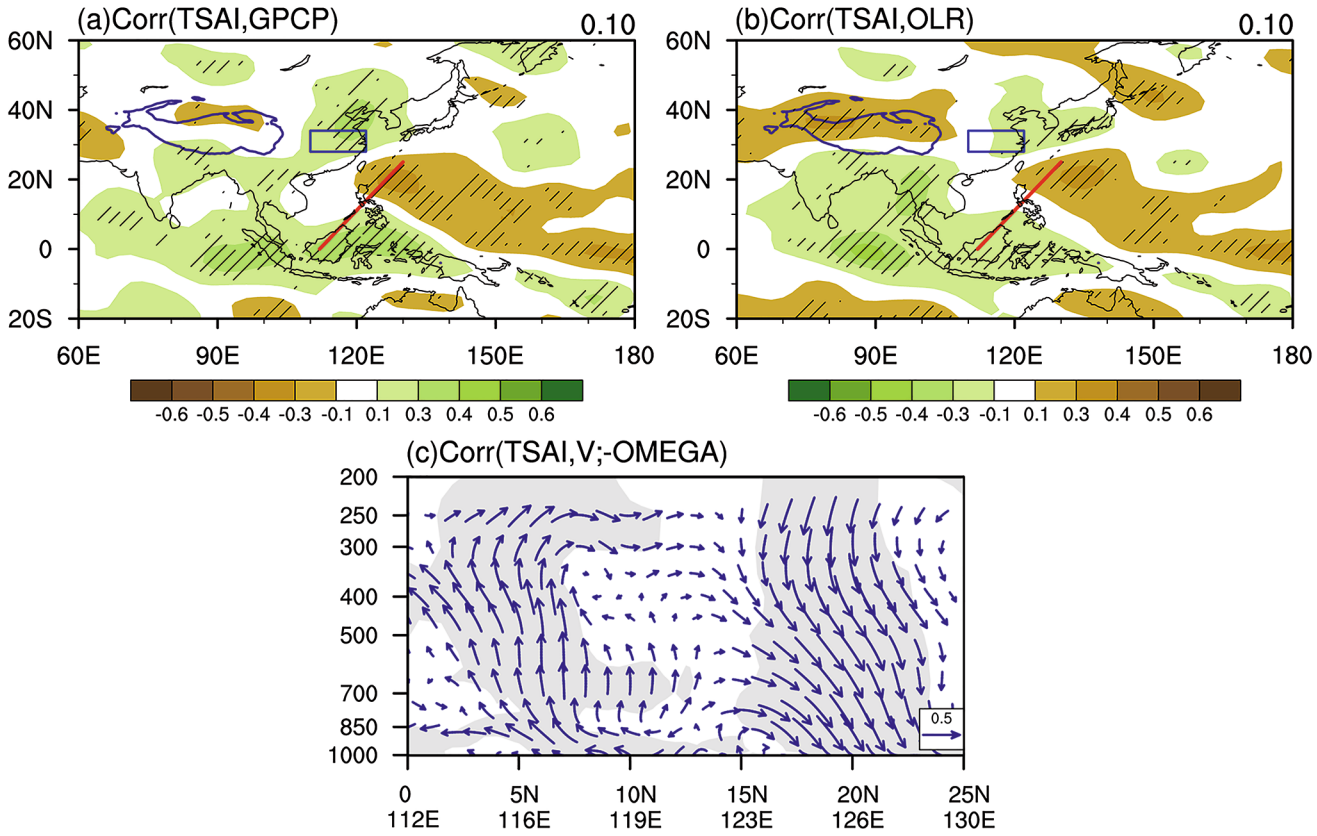

Fig. 5 (a) Correlation coefficients between the TSAI and rainfall. (b) Same as (a), but for OLR. Area exceeding the 0.1 significance level are highlighted by dashed black lines. (c) Correlation coefficients between the TSAI and circulation (vector) in cross section along the red oblique line in (b). Areas exceeding the 0.1 significance level are colored in gray shading

the Maritime Continent (Fig. 4c), the rainfall is strengthened (Fig. 5a) and the OLR is reduced (Fig. 5b), whereas the opposite occurs over the western North Pacific. The anomalous diabatic heating over the Maritime Continent and western North Pacific is linked via local Hadley circulation (Fig. 5c). On the one hand, the extratropical anomalous sinking motion and lower-level equatorward northerly wind in the anomalous local Hadley circulation favor less rainfall (Fig. 5a) and more OLR (Fig. 5b) to the east of Taiwan province and the Philippines. On the other hand, the feedback of diabatic heating in turn favors reinforcing of the meridional circulation, which is highly important for shaping the WNPAC (e.g., Wang et al. 2000; Neale and Slingo 2003; Li et al. 2020).

4.2 Linear baroclinic model experiment

The role of diabatic heating in the formation of the WNPAC is further examined using the LBM. Two experiments were conducted to investigate the anomalous diabatic heating induced by the positive TSAI phase. In the first experiment (Exp1), positive diabatic heating is prescribed over the Maritime Continent (Fig. 6a and b). In the second experiment (Exp2), negative diabatic heating is prescribed over the western North Pacific (Fig. 6d and e). The heating in Exp1 and Exp2 is given as the ideal elliptic pattern shown in Fig. 6b and d, respectively. The vertical structures are presented by a gamma curve with a peak at 0.45 sigma level to mimic the latent heat released in deep convection. The heating peak around 400 hPa is 1 K day^{-1} in Exp1 (Fig. 6a) and −1 K day^{-1} in Exp2 (Fig. 6d), which approximately equal an anomalous rainfall rate of 2 mm day^{-1} (Jiang et al. 2015).

Figure 6 shows the atmospheric circulation in response to heating over the Maritime Continent (Exp1) and cooling over the western North Pacific (Exp2). In Exp1 (Fig. 6a and b), the positive diabatic heating over the Maritime Continent induces a Gill-type response (Gill 1980). It is evident that a Rossby wave with a pair of cyclonic circulation appears to the west of heating and a Kelvin wave with easterlies appears to the east of the heating. The easterlies cover the area of 20°S–20°N (Fig. 6b). An anticyclonic wind shear centered over Japan to the south of 30° N is stimulated (Fig. 6b). However, compared with the reanalysis (Fig. 3b), the strength of this anticyclone in Fig. 6b is too weak and

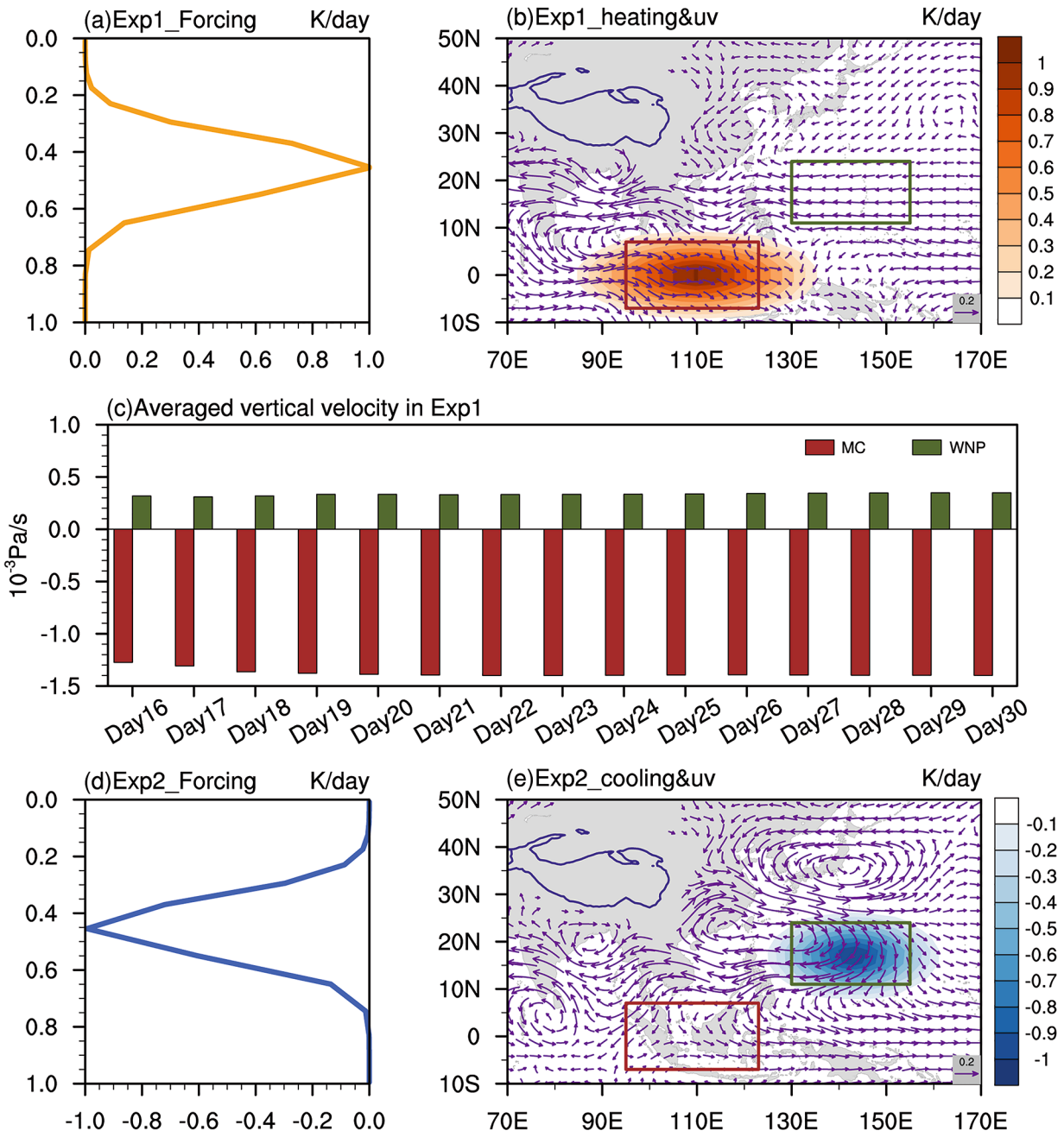

Fig. 6 (a) Vertical structure of the specified ideal diabatic heating over the Maritime Continent (units: K day^{-1}). (b) Horizontal distribution of the specified ideal diabatic heating over the Maritime Continent and the atmospheric response of horizontal wind (vector, units: m/s) at 850 hPa. (c) Area average of the vertical motion over the Maritime Continent (red shading; average of the red line area in (b)) and western North Pacific (green shading; average of the green line area in (b)). (d) and (e) are the same as (a) and (b), respectively, but for specified ideal diabatic cooling over the western North Pacific

the area is too small, which is not similar to the reanalysis (Fig. 3b). This is mainly because the atmospheric response decreases with latitude in the Gill solution (Gill 1980). This result suggests that the sole diabatic heating over the Maritime Continent can hardly directly trigger a realistic WNPAC.

However, it is evident that diabatic heating can change the local Hadley circulation, inducing an ascent motion over the Maritime Continent and a descent motion over the western North Pacific (Fig. 6c). This descent motion could contribute to the negative rainfall anomalies and diabatic cooling anomaly over the western North Pacific. In Exp2,

we show how the atmospheric circulation responds to the diabatic cooling over the western North Pacific.

In Exp2 (Fig. 6d and e), the diabatic cooling over the western North Pacific triggers a prominent anomalous anticyclone to the west of cooling. This atmospheric response in the subtropical high belt can be explained by the Sverdrup balance rule (Liu et al. 1999; Wu and Liu 2003), which is shown as follows:

$$\beta v \propto \frac{\partial Q}{\partial Z},$$

where β is the meridional gradient of the Coriolis parameter, v is the meridional wind, and $\frac{\partial Q}{\partial Z}$ is the vertical gradient of diabatic heating. Because the center of the anomalous diabatic cooling is above 850 hPa, the vertical gradient of diabatic heating is negative from the surface to 850 hPa. Subject to the Sverdrup balance, the northerly wind is triggered and the accompanied anticyclone thus forms to the west of the cooling center (Fig. 6e). Because the dry and cold northerly wind is conducive to less rainfall over the western North Pacific, the diabatic cooling associated with less rainfall, in turn, further strengthens the northerly wind. The anomalous WNPAC is consequently maintained and well developed under such a positive feedback mechanism. The well-developed anomalous WNPAC in Fig. 6e bears a close resemblance to the observation, suggesting that the local positive Sverdrup feedback effects of diabatic cooling over the western North Pacific on circulation play an important role in forming the anomalous WNPAC.

In summary, statistical analysis shows that TSA-SSTA could affect diabatic heating over the Maritime Continent by triggering a Gill response and anomalous Walker circulation. Diabatic heating over the Maritime Continent could induce diabatic cooling over the western North Pacific by stimulating local Hadley circulation. A sensitivity experiment (Exp1) reveals that diabatic heating alone over the Maritime Continent cannot lead to a realistic anomalous WNPAC. Further analysis reveals that local positive feedback mechanism (Sverdrup balance) between the anomalous diabatic cooling owing to reduced rainfall and the lower-level equatorward northerly wind plays an important role in the formation of the anomalous WNPAC, which is critical in the variation of the MOD.

4.3 AGCM sensitive experiment

The above results suggest a clear physical pathway in which TSA-SSTA affects the remote East Asian circulation. Two AGCM experiments were conducted based on CAM4 to further verify the mechanisms. The first AGCM experiment is a control run (CTL) driven by the climatological monthly mean SST. The second AGCM experiment is TSAI_POS, which is forced by 1.5 times the composite SST anomalies in the six strong positive TSAI years (larger than 1.0 standard deviation) plus the climatological SST from February to July over the TSA (25°S – 0°, 30°W–15°E). Both experiments are integrated over 20 years.

In general, the characteristics of the atmospheric response are basically consistent with the observations. The model captures the upper anomalous anticyclone circulation to the south of Japan (Fig. 7a) and the lower-level WNPAC (Fig. 7b). The WVF simulated by the model (Fig. 7c) is also similar with the reanalysis with convergence over the Maritime Continent and divergence over the western North Pacific (Fig. 2d).

The underlying mechanism in the sensitivity experiments is further shown in Figs. 8 and 9. The lower-level anomalous winds converge over the Atlantic and Maritime Continent, and diverge over the central Pacific (Fig. 8b). The upper level follows roughly the opposite scenario (Fig. 8a) with its counterparts at the lower level (Fig. 8b). The anomalous Walker circulation ascends over the TSA and Maritime Continent, and descends over the central Pacific (Fig. 8c). These results are consistent with the reanalysis shown in Fig. 4a and c. Figure 9 shows the composite difference of the rainfall and vertical circulation along the red line shown in Fig. 9a. The diabatic heating related to the rainfall over the Maritime Continent (Fig. 9a) stimulates local Hadley circulation, which favors anomalous ascending motion around 0°–10° N and descending motion around 15°–20° N (Fig. 9b). As a result, less rainfall occurs over the western North Pacific, which could initiate local positive Sverdrup feedback and eventually lead to a well-developed anomalous WNPAC. The abundant water vapor associated with the WVF (Fig. 7c) embedded in the WNPAC favors an earlier MOD. The mechanism revealed by the model is consistent with the statistical analysis, confirming that warm TSA-SSTA could contribute to an earlier MOD.

5 Conclusion and discussion

5.1 Conclusion

Meiyu is the major summer monsoon rainfall belt over the East Asia and exerts a strong impact on agriculture, socio-economic development, and societal activity. The MOD has received wide attention given its important implication for the prediction of the subsequent total rainfall and duration in the Meiyu season. The present study reveals the close interannual relationship between TSA-SSTA and the MOD, which has previously received little attention in the literature. The possible mechanism is examined using statistical

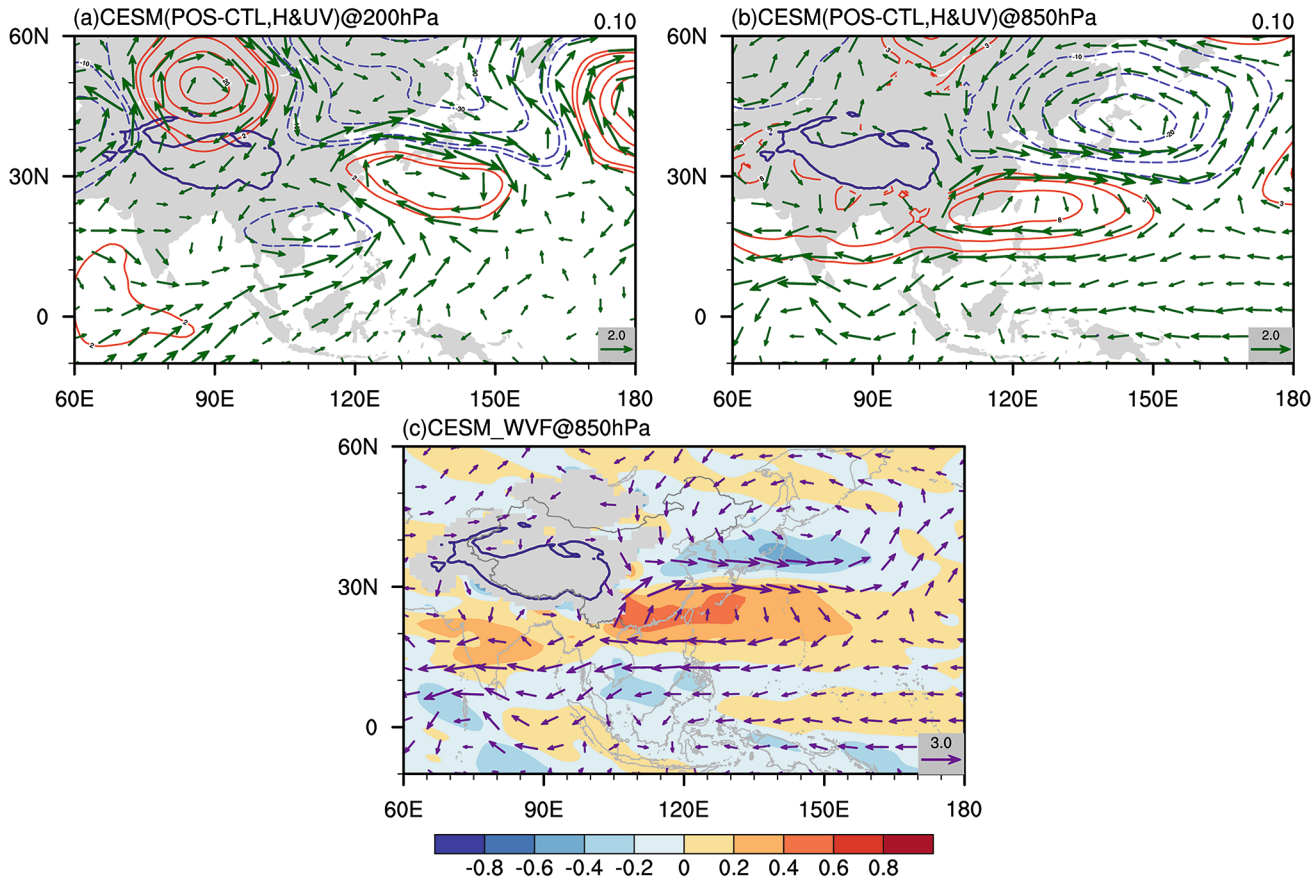

Fig. 7 Differences of (a) 200-hPa geopotential height (contours; units: gpm) and wind (vectors; units: m/s) between the TSAI_POS and CTL ensemble means in June. (b) Same as (a), but for 850 hPa. (c) Same as (a), but for an 850-hPa WVF (vector; units: 10^{-4} kg/(s · m · Pa)) and its divergence (shading; units: 10^{-9} kg/(s · m^2 · Pa))

analysis and numerical experiments, and the main conclusions are summarized as follows.

(1) The boreal spring TSA-SSTA as a driver independent of the spring ENSO could exert a significant influence on the Meiyu onset. A robust negative correlation between the spring TSAI and MOD is identified, with a correlation coefficient reaching −0.42 (passing the 0.01 significant level), which means that warm (cold) spring TSA-SSTA favor an earlier (later) MOD.

(2) The underlying mechanism by which TSA-SSTA affect the MOD is examined by reanalysis and numerical simulation. A schematic diagram showing this mechanism is presented in Fig. 10. In the positive TSAI phase (Fig. 10), warm TSA-SSTA could trigger a Gill response and change the Walker circulation along the equator. As a result, anomalous upward motion appears over the tropical Atlantic and Maritime Continent, and downward motion appears over the tropical central Pacific. Accordingly, more latent heating associated with the anomalous upward motion over the Maritime Continent enhances the local Hadley circulation, which could meridionally spread the tropical signal to the extratropic region. The descending branch in the local Hadley circulation around 20° N thus leads to lower-level equatorward northerly wind and an accompanied WNPAC to the west of the equatorward northerly wind. The abundant water vapor is consequently transported to the MLYRV by the anomalous WNPAC and thus favors an earlier MOD. In the negative TSAI phase, the situation is the opposite.

(3) The LBM experiments suggest that local positive Sverdrup feedback over the western North Pacific plays a fundamental role in maintaining the anomalous WNPAC. The anomalous equatorward northerly wind initiated by local Hadley circulation favors less latent heating over the western North Pacific. Subject to the Sverdrup constraint, less latent heating in turn strengthens the anomalous northerly wind. Under such positive

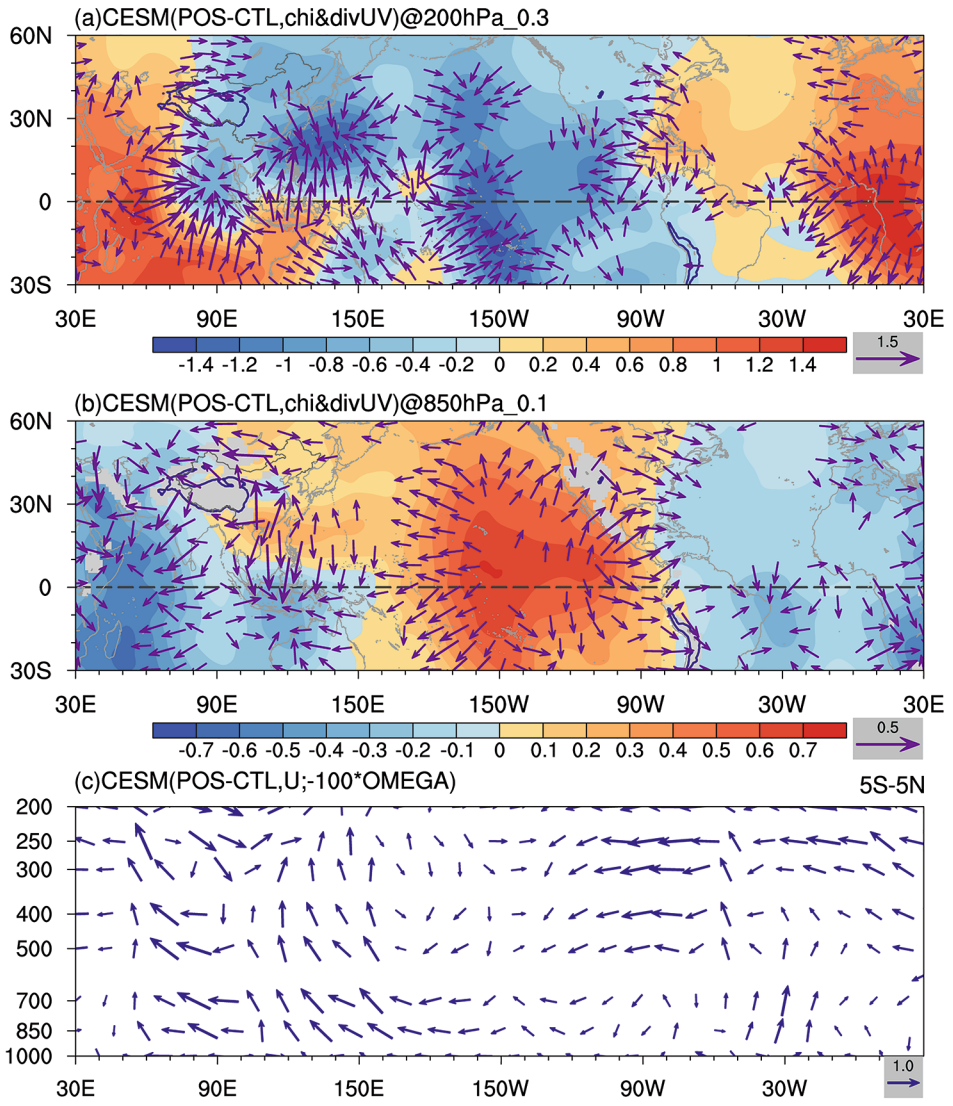

Fig. 8 Differences of variables between the TSAI_POS and CTL ensemble means. (a) 200-hPa velocity potential (shading; units: $10^6\ \mathrm{m}^2/\mathrm{s}$) and divergent wind (vectors; units: m/s; vectors with wind speed greater than 0.3 m/s are shown). (b) 850-hPa velocity potential (shading; units: $10^6\ \mathrm{m}^2/\mathrm{s}$) and divergent wind (vectors; units: m/s; vectors with wind speed greater than 0.1 m/s are shown). (c) 5°S–5°N mean zonal vertical circulation (arrows: u; $-100 \times \omega$)

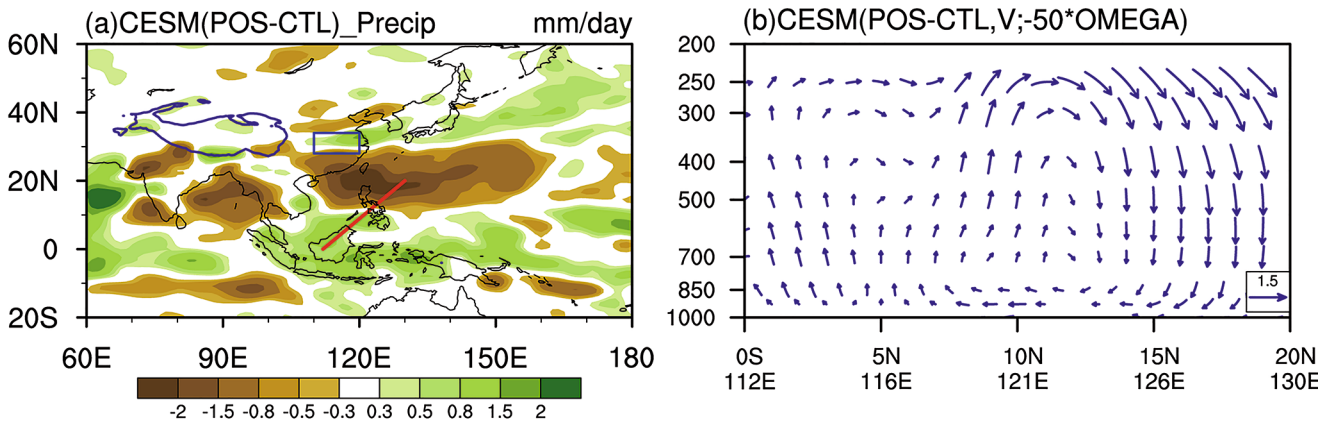

Fig. 9 Differences of (a) rainfall (units: mm/day) and (b) local meridional-vertical circulation (v; $-50 \times \omega$) along the red line shown in (a) between the TSAI_POS and CTL ensemble means

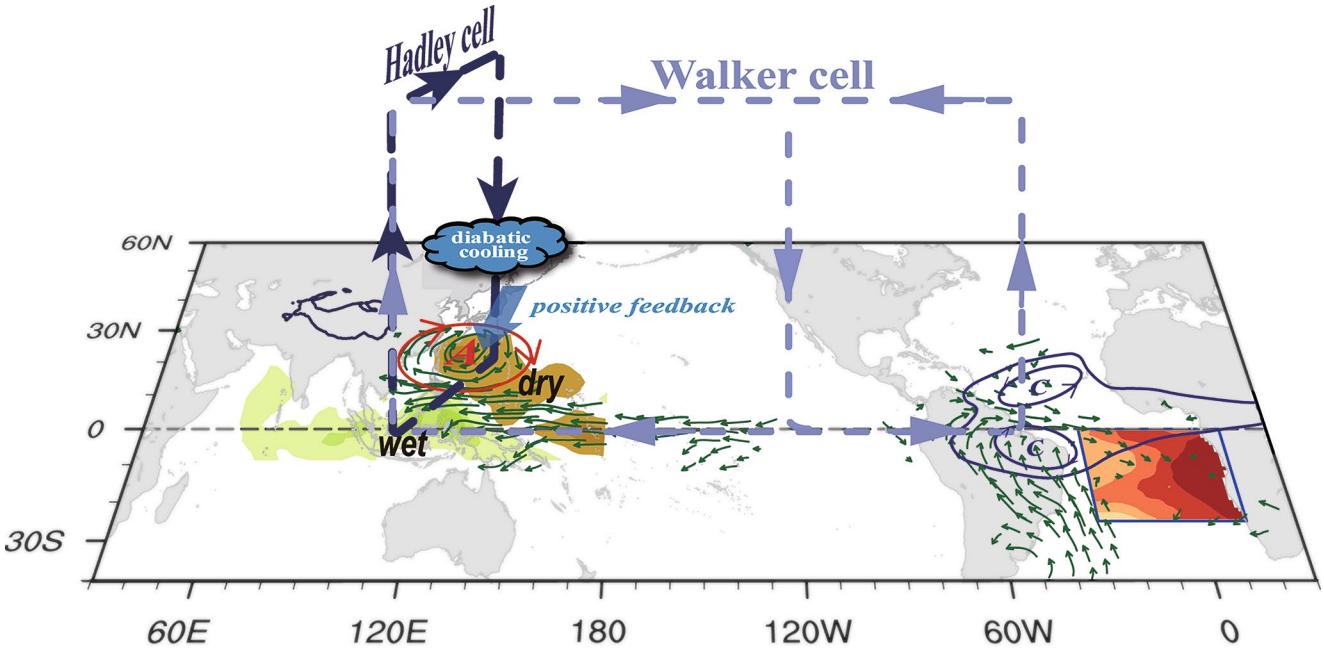

Fig. 10 Schematic diagram showing the interannual impact of spring TSA-SSTA on the MOD. The red shading over the TSA region indicates the anomalous warm spring TSA-SSTA. The horizontal green vectors overlain on the bottom map indicate anomalous 850-hPa wind in June from the reanalysis (identical to Fig. 4d). The red (navy blue) circle over the western North Pacific (tropical Atlantic) schematically indicates the anomalous anticyclone (Gill response). The shading over the western North Pacific and Maritime Continent denotes anomalous rainfall (identical to Fig. 5a). The light blue and dark blue vectors indicate Walker circulation and local Hadley circulation, respectively

feedback, the anomalous WNPAC to the west of the anomalous equatorward northerly wind could develop well.

5.2 Discussion

Besides the tropical route, there is also a possible pathway that the TSA trigger a Rossby wave propagating into the westerlies, dispersing downstream and affecting the south Asian high eventually (Jin and Huo 2018; Choi and Ahn 2019). This pathway deserves further study.

Previous studies have suggested that an eastward propagating teleconnection could transfer signals from the tropical Atlantic to the Indian Ocean (Kucharski et al. 2007, 2009). It is of interest to determine whether TSA-SSTA can affect East Asia via the Indian Ocean. Indeed, warm TSA-SSTA can produce a Kelvin wave with easterlies over the Indian Ocean as the response to the Gill mode (Kucharski et al. 2007, 2009). However, this Kelvin response to the east of the TSA is relatively weak in this study (Fig. 4), mainly because the propagation of the Kelvin wave dampens rapidly when coming across the Africa continent and because the easterlies over the Indian Ocean induced by the TSA-SSTA are offset by westerlies produced by the cold SST over the western Indian Ocean (Fig. 4d). The Indian Ocean pathway from which TSA-SSTA influence East Asia is therefore not prominent in this study.

In addition to TSA-SST, the MOD can also be affected by other factors. We calculate the correlation between the MODI and some well-understood factors (Fig. 11). The results in Fig. 11 suggest that the TSA, ENSO, and IOBM are the major predictors for the MOD anomaly. The two latter factors have been widely discussed in previous studies (Gao et al. 2006; Zhu et al. 2008; Wang et al. 2009; Yao et al. 2019). Other signals (e.g., NTA, NAO, TNA, PNA, DMI) are insignificantly correlated with the MODI. We further construct a regression equation using multiple linear regression analysis. Because the IOBM is largely determined by the preceding ENSO signal (Xie et al. 2009; Xie et al. 2016), we only consider the TSAI and Niño4 signal in the regression equation, which is given as:

$$MODI^{*} = -0.396 \times TSAI + 0.297 \times Niño4$$

.The partial regression coefficient magnitude for TSAI is larger than that for Niño4, thus this regression equation suggests that the connection between the MOD and TSA-SSTA is more intimate. The correlation coefficients between the MODI and reconstructed MODI* is −0.51, whereas the correlation coefficients between the MODI and single TSAI and Niño4 are − 0.42 and 0.32, respectively. The relationship

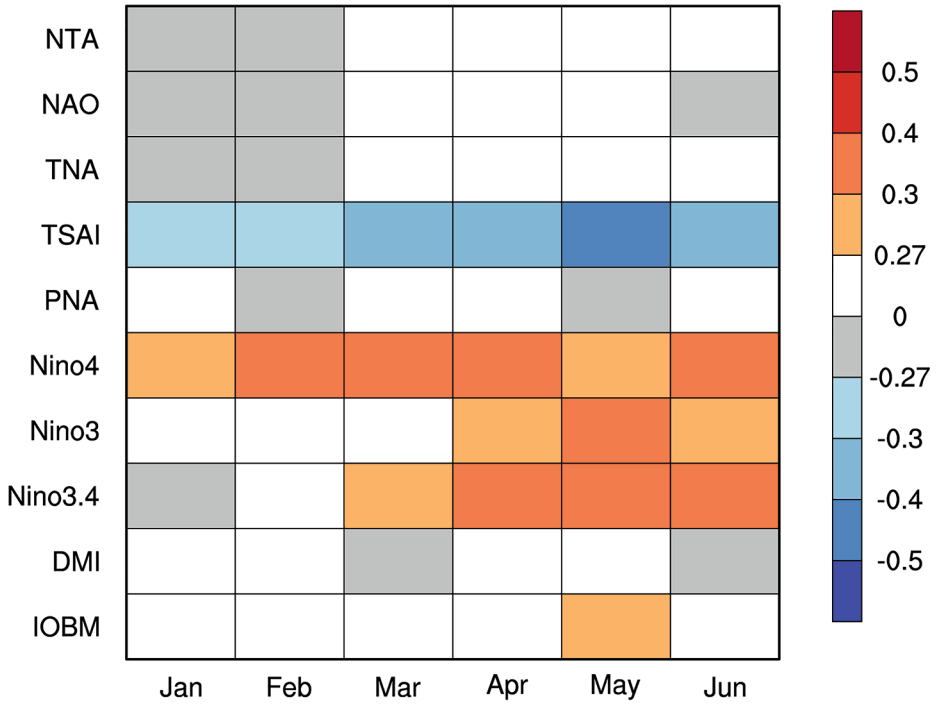

Fig. 11 Correlation coefficients between the MODI and some well-known preceding phenomena from January to June. Orange and blue denote that the correlations that exceed the 0.1 the significance level. (NTA: North Tripole Atlantic SST; NAO: North Atlantic Oscillation; TNA: Tropical Northern Atlantic Index; TSAI: Tropical Southern Atlantic Index; PNA: Pacific North American wave pattern; DMI: Indian Ocean dipole mode index; IOBM: Indian Ocean basin uniform mode index)

between the MODI and two-factor reconstruction is more intimate than either of the single factors, which indicates that the driving factors in the variation of the MOD are very complicated and still require further study. The clarification of these issues would advance the predictive skills of the MOD and associated extreme events over East Asia.

Acknowledgements The authors thank the three reviewers for their constructive and valuable suggestions and comments, which help us to substantially improve and strengthen the paper.

Author contributions Shaoyu Zhang contributed to the study conception and drafted the manuscript. Material preparation, data collection and analysis were also performed by Shaoyu Zhang. Yimin Liu and Chen Sheng contributed to the design of the present study. All authors edited and commented on the manuscript. All authors read and approved the final manuscript.

Funding This work was supported financially by the National Natural Science Foundation of China (Grant No. 42288101), the Strategic Priority Research Program of Chinese Academy of Sciences (Grant No. XDB40030204) and Guangdong Major Project of Basic and Applied Basic Research (Grant No. 2020B0301030004).

Data Availability The MERRA2 reanalysis dataset is available at https://disc.gsfc.nasa.gov/datasets?project=MERRA-2. The NOAA ERSSTv5 dataset is available at https://psl.noaa.gov/data/gridded/data.noaa.ersst.v5.html. The GPCP precipitation dataset is available at https://psl.noaa.gov/data/gridded/data.gpcp.html. Climate indices are obtained from https://psl.noaa.gov/data/climateindices/list/. The observational precipitation data among 824 stations in China provided by the Chinese Meteorological Information Center is available at http://data.cma.cn/en/?r=site/index.

Declarations The authors declare no conflicts of interest.

References

Adler RF et al (2018) The Global Precipitation Climatology Project (GPCP) Monthly Analysis (New Version 2.3) and a Review of 2017 Global Precipitation. Atmosphere 9. https://doi.org/10.3390/atmos9040138

Bjerknes J (1969) Atmospheric teleconnections from equatorial pacific. Monthly Weather Review 97:163–172

Chang P, Fang Y, Saravanan R, Ji L, Seidel H (2006) The cause of the fragile relationship between the Pacific El Nino and the Atlantic Nino. Nature 443:324–328. https://doi.org/10.1038/nature05053

Chen J, Wang X, Zhou W, Wang C, Xie Q, Li G, Chen S (2018) Unusual Rainfall in Southern China in Decaying August during Extreme El Nino 2015/16: Role of the Western Indian Ocean and North Tropical Atlantic SST. J Clim 31:7019–7034. https://doi.org/10.1175/jcli-d-17-0827.1

Chen XF, Zhao ZG (2000) Precipitation in Rainy Season in China: Prediction and Applications. China Meteorological Press, p 419

Choi YW, Ahn JB (2019) Possible mechanisms for the coupling between late spring sea surface temperature anomalies over tropical Atlantic and East Asian summer monsoon. Clim Dyn 53:6995–7009. https://doi.org/10.1007/s00382-019-04970-3

Ding QH (1992) Summer monsoon rainfalls in China. J Meteorol Soc Jpn 70:373–396

Ding QH, Liu JJ, Sun Y, Liu YJ, He JH, Song YF (2007) A Study of the Synoptic-Climatology of the Meiyu System in East Asia. Chin J Atmospheric Sci 31:1082–1101

Ding YH, Liang P, Liu YJ, Zhang YC (2020) Multiscale Variability of Meiyu and Its Prediction: A New Review. J Geophys Research-Atmospheres 125. https://doi.org/10.1029/2019jd031496

Enfield DB, Mestas-Nunez AM, Mayer DA, Cid-Serrano L (1999) How ubiquitous is the dipole relationship in tropical Atlantic sea surface temperatures? J Geophys Research-Oceans 104:7841–7848. https://doi.org/10.1029/1998jc900109

Gao H, Wang YG, He JH (2006) Weakening significance of ENSO as a predictor of summer precipitation in China. Geophys Res Lett 33. https://doi.org/10.1029/2005gl025511

Gao H, Yang S, Kumar A, Hu ZZ, Huang BH, Li YQ, Jha B (2011) Variations of the East Asian Mei-Yu and Simulation and Prediction by the NCEP Climate Forecast System. J Clim 24:94–108. https://doi.org/10.1175/2010jcli3540.1

Gill AE, SOME SIMPLE SOLUTIONS FOR HEAT-INDUCED TROPICAL CIRCULATION (1980) Q J R Meteorol Soc 106:447–462. https://doi.org/10.1002/qj.49710644905

Ham Y-G, Kug J-S, Park J-Y (2013) Two distinct roles of Atlantic SSTs in ENSO variability: North Tropical Atlantic SST and Atlantic Nino. Geophys Res Lett 40:4012–4017. https://doi.org/10.1002/grl.50729

Handoh IC, Bigg GR, Matthews AJ, Stevens DP (2006a) Interannual variability of the tropical Atlantic independent of and associated with ENSO: Part II. The South Tropical Atlantic. Int J Climatol 26:1957–1976. https://doi.org/10.1002/joc.1342

Handoh IC, Matthews AJ, Bigg GR, Stevens DP (2006b) Interannual variability of the tropical Atlantic independent of and associated with ENSO: Part I. The North Tropical Atlantic. Int J Climatol 26:1937–1956. https://doi.org/10.1002/joc.1343

Hersbach H et al (2020) The ERA5 global reanalysis. Q J R Meteorol Soc 146:1999–2009. https://doi.org/10.1002/qj.3803

Hong CC, Chang TC, Hsu HH (2014) Enhanced relationship between the tropical Atlantic SST and the summertime western North Pacific subtropical high after the early 1980s. J Geophys Research-Atmospheres 119:3715–3722. https://doi.org/10.1002/2013jd021394

Hu YJ, Zhu YM, Zhong Z, Ha Y (2014) New Predictors and a Statistical Forecast Model for Mei-Yu Onset Date in the Middle and Lower Reaches of the Yangtze River Valley. Weather Forecast 29:654–665. https://doi.org/10.1175/waf-d-13-00109.1

Huang BH, Schopf PS, Shukla J (2004) Intrinsic ocean-atmosphere variability of the tropical Atlantic Ocean. Journal of Climate 17:2058-2077. https://doi.org/10.1175/1520-0442(2004)017<2058:Iovott>2.0.Co;2

Huang B et al (2017) Extended Reconstructed Sea Surface Temperature, Version 5 (ERSSTv5): Upgrades, Validations, and Intercomparisons. J Clim 30:8179–8205. https://doi.org/10.1175/jcli-d-16-0836.1

Huang QL, Wang LJ, Li Y, He JH (2012) Determination of the onset and ending of regional Meiyu over Yangtze-Huaihe River Valley and its characteristics. J Trop Meteorol 28:749–756

Hunke EC, Lipscomb WH (2008) The Los Alamos sea ice model documentation and software user's manual version 4.0. Los Alamos National Laboratory Tech Rep:LA-CC-06-012

Ishii M, Shouji A, Sugimoto S, Matsumoto T (2005) Objective analyses of sea-surface temperature and marine meteorological variables for the 20th century using icoads and the Kobe collection. Int J Climatol 25:865–879. https://doi.org/10.1002/joc.1169

Jiang X, Li Y, Yang S, Shu J, He G (2015) Interannual variation of mid-summer heavy rainfall in the eastern edge of the Tibetan Plateau. Clim Dyn 45:3091–3102. https://doi.org/10.1007/s00382-015-2526-0

Jiang ZH, Ren W, Liu ZY, Yang H (2013) Analysis of water vapor transport characteristics during the Meiyu over the Yangtze-Huaihe River valley using the Lagrangian method. Acta Meteorologica Sinica 71:295–304

Jin DC, Huo LW (2018) Influence of tropical Atlantic sea surface temperature anomalies on the East Asian summer monsoon. Q J R Meteorol Soc 144:1490–1500. https://doi.org/10.1002/qj.3296

Kubota H, Kosaka Y, Xie SP (2016) A 117-year long index of the Paci c-Japan pattern with application to interdecadal variability.International Journal of Climatology36

Kucharski F, Bracco A, Yoo JH, Molteni F (2007) Low-frequency variability of the Indian monsoon-ENSO relationship and the tropical atlantic: The "Weakening" of the 1980s and 1990s. J Clim 20:4255–4266. https://doi.org/10.1175/jcli4254.1

Kucharski F, Bracco A, Yoo JH, Tompkins AM, Feudale L, Ruti P, Dell'Aquila A (2009) A Gill-Matsuno-type mechanism explains the tropical Atlantic influence on African and Indian monsoon rainfall. Q J R Meteorol Soc 135:569–579. https://doi.org/10.1002/qj.406

Li H, He SP, Fan K, Wang HJ (2019a) Relationship between the onset date of the Meiyu and the South Asian anticyclone in April and the related mechanisms. Clim Dyn 52:209–226. https://doi.org/10.1007/s00382-018-4131-5

Li Y, Deng Y, Yang S, Zhang HA (2018) Multi-scale temporospatial variability of the East Asian Meiyu-Baiu fronts: characterization with a suite of new objective indices. Clim Dyn 51:1659–1670. https://doi.org/10.1007/s00382-017-3975-4

Li Y, Sen Gupta A, Taschetto AS, Jourdain NC, Di Luca A, Done JM, Luo J-J (2020) Assessing the role of the ocean-atmosphere coupling frequency in the western Maritime Continent rainfall. Clim Dyn 54:4935–4952. https://doi.org/10.1007/s00382-020-05266-7

Li Z, Chen c, Zeng G, Deng W, Wu L (2019b) Characteristics of North tropical Atlantic SSTA in spring and its relationship with mid-summer precipitation in China. J Trop Meteorol 35:756–766

Liebmann B, Smith CA (1996) Description of a complete (interpolated) outgoing longwave radiation dataset. Bull Am Meteorol Soc 77:1275–1277

Liu B, Yan Y, Zhu C, Ma S, Li J (2020a) Record-Breaking Meiyu Rainfall Around the Yangtze River in 2020 Regulated by the Subseasonal Phase Transition of the North Atlantic Oscillation. Geophys Res Lett 47. https://doi.org/10.1029/2020gl090342

Liu XL, Liu YM, Wang XC, Wu GX (2020b) Large-Scale Dynamics and Moisture Sources of the Precipitation Over the Western Tibetan Plateau in Boreal Winter. J Geophys Research-Atmospheres 125. https://doi.org/10.1029/2019jd032133

Liu YM, Wu GX, Liu H, Liu P (1999) The effect of spatially nonuniform heating on the formation and variation of subtropical high. Part III: Condensation heating and South Asian high and western Pacific subtropical high. Acta Meteor Sin 57:327–338

Lu RY, Oh JH, Kim BJ, Baek HJ, Huang RH (2001) Associations with the interannual variations of onset and withdrawal of the Changma. Advances in Atmospheric Sciences 18:1066-1080. https://doi.org/10.1007/s00376-001-0023-3

Neale RB, Richter J, Park S, Lauritzen PH, Vavrus SJ, Rasch PJ, Zhang M (2013) The Mean Climate of the Community Atmosphere Model (CAM4) in Forced SST and Fully Coupled Experiments. J Clim 26:5150–5168

Ninomiya K, Muraki H (1986) Large scale circulation over East Asia during Baiu period of 1979. J Meteorol Soc Jpn 64:409–429

Oleson KW et al (2010) Technical description of version 4.0 of the Community Land Model (CLM). NCAR Technical Note NCAR/TN-478 + STR, p 266

Qiu D, Xu H, Deng J, Ma J (2021) Different impacts of spring tropical Atlantic SST anomalies on Eurasia spring climate during the periods of 1970–1995 and 1996–2018. https://doi.org/10.1016/j.atmosres.2021.105494. Atmospheric Research 253

Rienecker MM et al (2011) MERRA: NASA's Modern-Era Retrospective Analysis for Research and Applications. J Clim 24:3624–3648. https://doi.org/10.1175/jcli-d-11-00015.1

Rong X, Zhang R, Li T (2010) Impacts of Atlantic sea surface temperature anomalies on Indo-East Asian summer monsoon-ENSO relationship. Chin Sci Bull 55:2458–2468. https://doi.org/10.1007/s11434-010-3098-3

Saji NH, Goswami BN, Vinayachandran PN, Yamagata T (1999) A dipole mode in the tropical Indian Ocean. Nature 401:360–363. https://doi.org/10.1038/43855

Sheng C, Wu GX, He B, Liu YM, Ma TT (2022) Linkage between cross-equatorial potential vorticity flux and surface air temperature over the mid-high latitudes of Eurasia during boreal spring. Clim Dyn. https://doi.org/10.1007/s00382-022-06259-4

Smith RD, Gent P (2010) The Parallel Ocean Program (POP) reference manual. Los Alamos National Lab Technical Report:141

Stein AF, Draxler RR, Rolph GD, Stunder BJB, Cohen MD, Ngan F, NOAA'S HYSPLIT ATMOSPHERIC TRANSPORT AND DISPERSION MODELING SYSTEM (2015) Bull Am Meteorol Soc 96:2059–2077. https://doi.org/10.1175/bams-d-14-00110.1

Tao SY, Chen LX (1987) A review of recent research on the East Asian summer monsoon in China.Review in Monsoon Meteorology,Oxford Univ Press:60–92

Trenberth KE (1998) Atmospheric moisture residence times and cycling: Implications for rainfall rates and climate change. Climatic Change 39:667–694. https://doi.org/10.1023/a:1005319109110

Trenberth KE (1999) Atmospheric moisture recycling: Role of advection and local evaporation. Journal of Climate 12:1368–1381. https://doi.org/10.1175/1520-0442(1999)012<1368:Amrroa>2.0.Co;2

Wang B, Wu RG, Fu XH (2000) Pacific-East Asian teleconnection: how does ENSO affect East Asian climate? Journal of Climate 13:1517–1536. https://doi.org/10.1175/1520-0442(2000)013<1517:Peathd>2.0.Co;2

Wang J, He JH, Liu XF, Wu BG (2009) Interannual variability of the Meiyu onset over Yangtze-Huaihe River Valley and analyses of its previous strong influence signal. Chin Sci Bull 54:687–695

Wang LJ, He JH, Si D, Wen M, Zhong SS (2010) Analysis of Impacts of Northeast Cold Vortex Processes on Meiyu Rainfall Period over Yangtze-Huaihe River Basin. Trans Atmospheric Sci 33:89–97

Wang ZR, Qian YF (2005) The Affection of Sea-surface Temperature anomaly to Meiyu Onset Date of Yangtse-Huaihe River Valley. J Appl Meteorological Sci 16:193–204

Watanabe M, Kimoto M (2000) Atmosphere-ocean thermal coupling in the North Atlantic: A positive feedback. Q J R Meteorol Soc 126:3343–3369. https://doi.org/10.1002/qj.49712657017

Watanabe M, Jin FF (2003) A moist linear baroclinic model: Coupled dynamical-convective response to El Nino. Journal of Climate 16:1121-1139. https://doi.org/10.1175/1520-0442(2003)16<1121:Amlbmc>2.0.Co;2

Wei FY, Zhang JJ (2004) Climatic variation of Meiyu in the middle-lower reaches of Changjiang River during 1885–2000. J Appl Meteorological Sci 15:313–321

Wu GX, Liu YM (2003) Summertime quadruplet heating pattern in the subtropics and the associated atmospheric circulation. Geophys Res Lett 30. https://doi.org/10.1029/2002gl016209

Xie SP, Hu KM, Hafner J, Tokinaga H, Du Y, Huang G, Sampe T (2009) Indian Ocean Capacitor Effect on Indo-Western Pacific Climate during the Summer following El Nino. J Clim 22:730–747. https://doi.org/10.1175/2008jcli2544.1

Xie SP, Kosaka Y, Du Y, Hu KM, Chowdary J, Huang G (2016) Indo-western Pacific ocean capacitor and coherent climate anomalies in post-ENSO summer: A review. Adv Atmos Sci 33:411–432. https://doi.org/10.1007/s00376-015-5192-6

Xu HM, He JH, Dong M (2001) Interannual Variability of the Meiyu Onset and Its Association with North Atlantic Oscillation and SSTA over North Atlantic. Acta Meteorologica Sinica 59:694–706

Yang H, Jiang Z, Liu Z (2014) Analysis of climatic characteristics of water vapor transport based on the Lagrangian method: A comparison between Meiyu in the Yangtze – Huaihe River region and the Huaibei rainy season. Chin J Atmospheric Sci 38:965–973

Yao YH, Lin H, Wu QG (2019) Linkage between Interannual Variation of the East Asian Intraseasonal Oscillation and Mei-Yu Onset. J Clim 32:145–160. https://doi.org/10.1175/Jcli-D-17-0873.1

Yuan CX, Yang MZ (2020) Interannual Variations in Summer Precipitation in Southwest China: Anomalies in Moisture Transport and the Role of the Tropical Atlantic. J Clim 33:5993–6007. https://doi.org/10.1175/jcli-d-19-0809.1

Zhao Y, Duan AM, Wu GX (2018) Interannual Variability of Late-spring Circulation and Diabatic Heating over the Tibetan Plateau Associated with Indian Ocean Forcing. Adv Atmos Sci 35:927–941. https://doi.org/10.1007/s00376-018-7217-4

Zhao ZG (1996) Impact of El Nino Events on Atmospheric Circulations in the Northern Hemisphere and Precipitation in China.Scientia Atmospherica Sinica 20

Zhou XY, Liu F, Wang B, Xiang BQ, Xing C, Wang H (2019) Different responses of East Asian summer rainfall to El Nino decays. Clim Dyn 53:1497–1515. https://doi.org/10.1007/s00382-019-04684-6

Zhu X, Wu Z, He J (2008) Anomalous Meiyu onset averaged over the Yangtze River Valley. Theoret Appl Climatol 94:81–95. https://doi.org/10.1007/s00704-007-0347-8